ELSEVIER

Contents lists available at ScienceDirect

Materials Science & Engineering A

journal homepage: www.elsevier.com/locate/msea



Dissimilar joining of Cu₄₆Zr₄₆Al₈ metallic glass and 304 stainless steels through liquid-solid casting

Yu Zhang ^{a,b}, Luyao Li ^b, Xin Li ^b, Wenxin Wen ^b, Yong Xiao ^{a,*}, Dan Li ^a, Jiang Ma ^{b,**}

ARTICLE INFO

Keywords: Metallic glasses 304 stainless steels Liquid-solid casting Dissimilar joining

ABSTRACT

Humans have long pursued metallic materials with excellent properties. Metallic glasses (MGs) have superior mechanical performance due to their amorphous structure, but suffer from brittleness and size limitations. Joining, especially dissimilar joining, offers a solution to these issues. Here, through a liquid-solid casting process, we successfully joined $Cu_{46}Zr_{46}Al_8$ MGs and 304 stainless steels together without cracks and voids. A solid metallurgical bonding is achieved at the atomic level in the interface. The transition layer has a thickness of around 40 nm at the interface with elements diffusion and oxygen enrichment of 30 %. The joining quality was assessed through compression and tensile testing. The compression strength can reach 1461 MPa, achieving 97 % of the as-cast $Cu_{46}Zr_{46}Al_8$ MG. In addition, the tensile strength can reach 404 MPa before fracture after a strain of 12.6 %. Our results demonstrated that the liquid-solid casting process completes material preparation and dissimilar joining of MGs and alloys simultaneously, obtaining improved performance through reasonably designing the state of joined metal.

1. Introduction

Researchers have long sought to design and produce metallic materials with outstanding properties. To keep up with the demands of the rapidly advancing industrial sector, a variety of new materials have been developed [1–4]. Bulk metallic glass (BMG), as a novel material, has become a hot topic in materials research over the past few decades [5–9]. Due to the disordered arrangement at the atomic scale, it exhibits a lot of excellent qualities such as ultrahigh fracture strength [10,11], Co-based MG has reported a high strength of about 4.7 GPa [12], unique soft magnetic properties [13], superior elastic limit [14], and exceptional resistance to corrosion and wear [15,16] and so on. Many potential commercial values are waiting to be explored. However, to obtain the disordered atomic structure, a sufficiently high cooling rate (>10 3 K/s) is usually needed, the size limitation of MG restricted by the glass forming ability (GFA), remains the biggest restriction for their engineering applications.

Joining, as a traditional method of welding materials, has established itself as a reliable technique for combining metallic glasses to raise the critical size. Previous works have demonstrated the success of numerous

joining techniques that joined MGs in several alloy systems. Joining techniques can be classified into two primary groups based on the alloy's solid or liquid state at the moment of joining. One is a liquid-state process that uses lasers [17], electron beams [18], pulse currents [19], and arc welding [20], the other is a solid-state process that uses ultrasonic joining techniques [21], friction [22], explosions [23,24], and thermoplastic deformation [25]. Metallic glass can be quickly and solder-free joined using ultrasonic joining, which takes advantage of the quick surface dynamics of amorphous alloys [21,26,27]. What's more, this ultrasonic joining is also described as a technique for joining various metallic glass kinds under liquid environments like liquid nitrogen, alcohol, seawater, and water [28].

In addition to increasing the size of MG, the dissimilar joining of MGs with pure metal and alloys was also worth investigating with the advantages of establishing connections between materials with certain functions to expand their engineering applications. Aluminum alloys, acknowledged as a kind of premium material that is only surpassed by steel, were successfully joined with $\rm Zr_{55}Cu_{30}Ni_5Al_{10}$ by using Ar ion irradiation [29], the successful application of electron beam brazing to $\rm Zr_{62}Al_{13}Ni_7Cu_{18}$ bulk metallic glass plate to pure Ti metal has produced

E-mail addresses: yongxiao@whut.edu.cn (Y. Xiao), majiang@szu.edu.cn (J. Ma).

^a School of Materials Science and Engineering, Wuhan University of Technology, 430070, Wuhan, China

^b Shenzhen Key Laboratory of High Performance Nontraditional Manufacturing, College of Mechatronics and Control Engineering, Shenzhen University, 518060, Shenzhen, China

^{*} Corresponding author.

^{**} Corresponding author.

a 2 mm thick plate [18]. Kim et al. [30] successfully joined 2 mm thick $\rm Zr_{41}Be_{23}Ti_{14}Cu_{12}Ni_{10}$ BMG plate to stainless steel STS316L by using electron beam welding, but the results shown a reaction region at the interface was unavoidable, and a large amount of crystallization was found near the interface. MGs are sensitive to temperature rise, but the majority of methods need a heat source to melt alloy which will lead to inevitable crystallization and even a vacuumed environment needed to avoid oxidation, a quick and innovative techniques for dissimilar joining are desperately needed.

Here, we conduct experiments and try to join Cu46Zr46Al8 metallic glass with 304 stainless steels by using a liquid-solid casting method. These Zr-based MGs reported possess high glass forming ability which is a key factor in implementing the liquid-solid casting method, and its industrial value under excellent mechanical properties. 304 stainless steels are the widely utilized low-priced alloys in the industrial, furniture decoration, culinary, and medical industries [31,32], during the process, the high-temperature molten metal liquid was poured directly into a copper mold with a pre-positioned SUS304 rod. Rapid cooling enabled the liquid metal to maintain its amorphous structure and bound to SUS304 as a single unit, a higher cooling rate can prevent crystallization and then increase the quality of the joint. The interface showed no voids or cracks between MG and SUS304 and a robust metallurgical bonding at the atomic level was observed, indicating a high-quality joining. What's more, the joined samples exhibit remarkable strengths for a dependable dissimilarity joining process, with a compression strength of 1461 MPa and tensile strength of 404 MPa. Our results demonstrated this is an easy and reliable way to achieve dissimilar joining of metallic glass to steels, which has potential engineering applications.

2. Experimental method

2.1. Sample preparation

The $\text{Cu}_{46}\text{Zr}_{46}\text{Al}_8$ (at.%) composition was used for this experiment. All elements were manufactured from pure metals with a purity higher than 99.99 %. The master alloy was melted roughly 5 times in a vacuum arc melting furnace with argon gas shielding to ensure the uniform distribution of the elements. 304 stainless steel (wt.%: C, 0.08; Mn, 2.0; Si, 1.0; P, 0.04; S,0.03; Cr, 19.0; Ni, 9.0) was purchased directly as a commercial product, rob with diameter of 1 mm and sheet with thickness of 1.5 mm were carefully polished by 2000# sandpaper, 10 min ultrasonic cleaning conducted to make sure a bright and clean surface.

2.2. Structure characterization

Scanning electron microscopy (SEM; Quanta FEG 450, FEI) was used to observe the joined quality from the joined interface, it works under a backscatter mode, the operating voltage is 30 kV and the magnification is 400 times. The phase structure along the interface was investigated by Cu-Kα radiation X-ray diffraction (XRD, Rigaku MiniFlex 600), the wavelength of the X-ray is 0.154 nm, and the rated power is 600 W, the scan angle is from 20° to 90° . TEM samples with a length of 5 μm , and width of 2 µm were prepared from the interface by using a FEI Scios SEM/FIB dual beam system. The microstructure of the joined interface was analyzed by a double spherical-aberration corrected transmission electron microscope (TEM; FEI, Netherlands), and the phase structure near the interface was further confirmed by selected electron diffraction (SEAD). The TEM-equipped energy-dispersive spectroscopy (EDS) was used to measure the distribution of elements from the interface, and a line scan was conducted to measure the variation of elements along a specific line.

2.3. Mechanical properties tests

The variation of hardness along the interface was verified by a

nanoindentation instrument (TI 980, Bruker, Germany) using a Berkovich triangular pyramid indenter, with a maximum load of 10 mN, intervals of each test point was 1 μm , each point test five times and take the average. The engineering strain-stress curve was measured by a mechanical testing machine (UMT-5105, SanSi, China), the test was conducted under room temperature with a strain rate of $\sim \! \! 1 \times 10^{-4}$ strain rate, a laser non-contact extensometer (500LC, Tinius Olsen, China) was used to increase the accuracy of strain.

2.4. Liquid-solid casting

The schematic diagram of the proposed solid-liquid casting approach is illustrated in Fig. 1(a). A copper mold with a through hole diameter of 3 mm in the middle was used to provide a high cooling rate. In the beginning, the 304 stainless steel (Hereinafter called SUS304) rod 70 mm in length and 1 mm in diameter was attached in the mold's center, after that, the molten state liquid master alloy was die-cast into the mold cavity rapidly driven by pressure difference.

2.5. Sample preparation for mechanical test

The mentioned joined rob with a 3 mm diameter was cut by the diamond cutting machine, the length is 6 mm, resulting in a 2 height-to-diameter ratio for compressing test. Some T-shaped groove was prefabricated on the joint of USU 304, the height of the groove is 0.6 mm, the long side is 0.8 mm and the short side is 0.3 mm. Then placed the SUS 304 mold into the copper mold, and the molten CuZrAl metal liquid suck into the mold quickly due to the pressure difference adjusted by the pressure control valve, the molten liquid filled the T-shaped groove and bonded together. Bone-like standard tensile piece (see it in Fig. 5(c)) prepared for tensile test.

3. Results and discussions

3.1. Display of joined samples

The photo of the processed sample is shown in Fig. 2(b), it has no visual distinction from regular metallic glass rob from this view. However, the difference can be seen from the circular cross-section as shown in Fig. 1(c), different lining colors indicate it consists of two different materials, three markers #1, #2, and #3 represent 304 stainless steel, the interface between them and metallic glass matrices respectively. The interface represented by the gray border has been magnified to Fig. 1(d), a clear joining line without any voids and cracks between SUS304 and MG matrix revealed that the molten Cu₄₆Zr₄₆Al₈ MG showed good joinability with the SUS304. To assess the effect of inserted material on the cooling rate and phase evolution near the interface. Fig. 1(e) shows the XRD patterns of three crucial points marked#1, #2, and #3 in Fig. 1 (c), the distance between these three marks is 500 µm. Line #1 shows a main γ -Fe austenite phase, the peak position and phase are the same as reported [33], so this is a typical SUS304 diffraction pattern. Diffraction pattern #3 shows a broad diffuse peak indicating that there is only an amorphous phase, which means the forming of an amorphous structure will not be impacted by the inclusion of stainless steel. Moreover, the majority of diffraction pattern #2 is still composed of the broad diffuse peaks along with the γ -Fe austenite phase mentioned before without any new peaks, which indicates that no new phases were generated during the joining process.

To deeply investigate the interface of the joined region, the continuous nanoindentation hardness measurements started from the SUS304 matrix with an interval of 1 μm were conducted. Results are demonstrated in Fig. 1(f), From the beginning, the hardness values float from 6 GPa. Following, the values began to rise steadily at 2 μm away from the interface, as the test continued, the values reached 7.8 GPa and remained constant at this level, resulting in a transition zone of approximately 4.5 μm was observed.

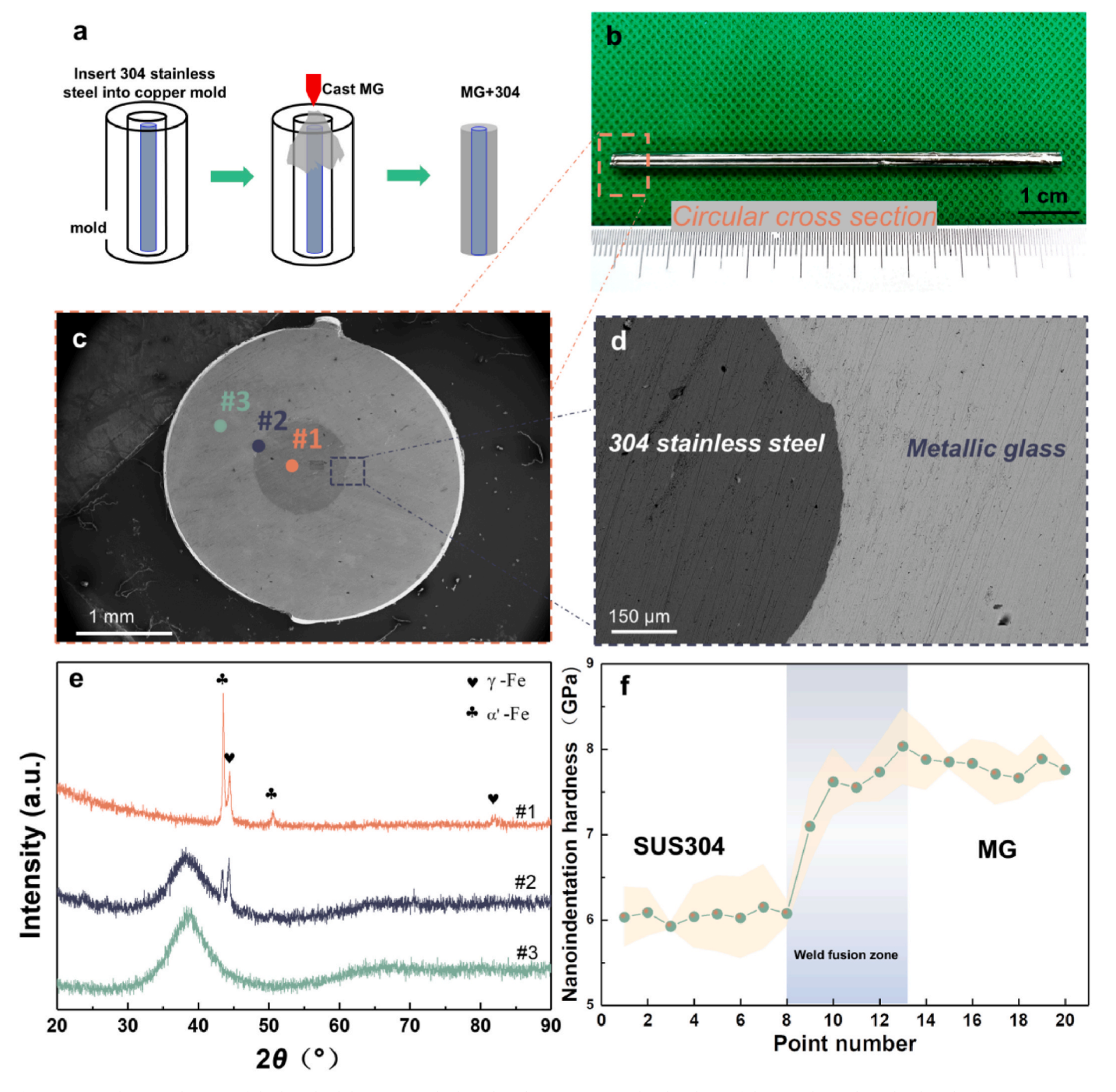


Fig. 1. (a) A schematic diagram of the liquid-solid casting method used in this experiment. (b) The photo of the joined sample with a length of 70 mm. (c) SEM morphology from circular cross-section. (d) Enlarged SEM morphology belongs to the interface of joined SUS304 and MG. (e) X-ray patterns of #1, #2, and #3 marked in (c). (f) Nanoindentation hardness results across the interface of SUS304 and MG with an interval of 1 μ m.

3.2. Elemental distribution along the interface

Based on the mechanical tests above, within a specific range, one hardness values changing region can be seen, which indicates that there should be a transition zone at the interface. The High-Angle Annular Dark Field (HADDF) image form interface is demonstrated in Fig. 2(a), the presence of the transition layer can be seen through the contrast in the image, the dark area mimicked by white lines is joined region, the upper and lower sections from joined region correspond to the SUS304 and MG matrix, respectively.

An Elemental Distribution investigation on the joined region was conducted to assist in a better understanding of the joining mechanism.

As is well known, the main elements consisting of SUS304 are Fe, Ni, and Cr [34], besides, the main elements consisting of MG used in the experiment are Cu, Zr, and Al. Fig. 2(a) displays the EDS maps of these six elements in addition to oxygen. Each color represents one element, and the density of the color represents the concentration of this element. The black areas in the image indicate that this element is non-existent. To better describe element distribution across joined regions, a line scan along the blue arrow in the HADDF image to describe the concentration variations of these major elements across the interface are illustrated in Fig. 2(b). The elements contained in the solid solution layer between MG and SUS304 are spread in a continuous gradient. The length of the transition elements region represents the width of this solid



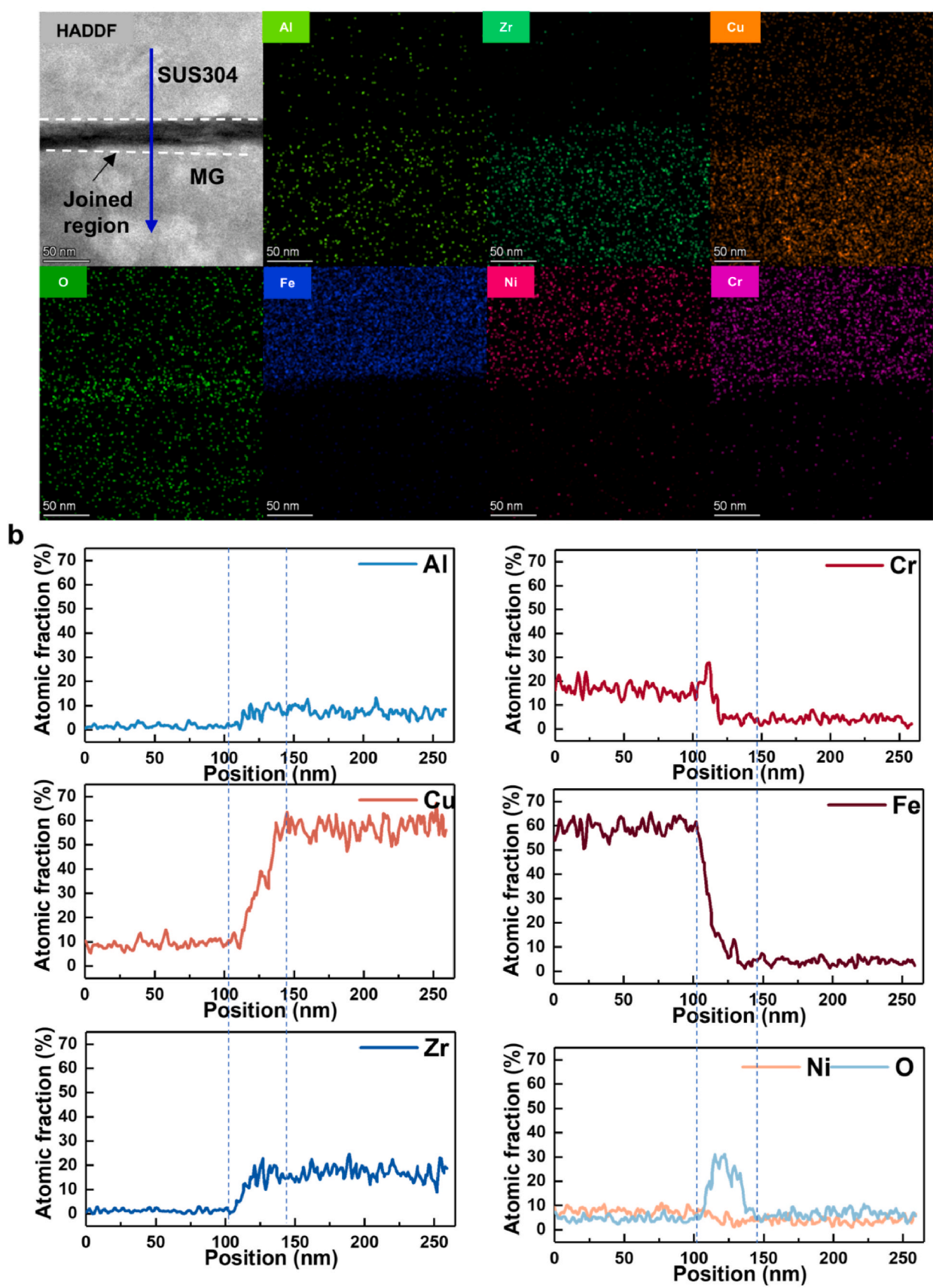


Fig. 2. (a) Energy dispersive spectroscopy (EDS) maps showing elements distribution from the interface of SUS304 and MG. (b) The line scan results of each element along the blue arrow in (a). (For interpretation of the references to color in this figure legend, the reader is referred to the Web version of this article.)

solution layer, it is measured about 40 nm. The length of the joint is shorter than some other approaches which need filler metals, Kim et al. [35] weld Cu-based metallic glass with carbon steel using Zn-Ag-Al as filler, the interface is about 10 μm . Additionally, the diffusion thickness of the three elements from the MG side is higher than SUS304, perhaps because of the metal liquid's higher temperature, higher internal energy, and improved diffusion rate in its molten condition. In addition, The oxygen content rapidly increases in the solid solution layer, reaching a maximum value of 30 %, which indicates that the formation of the solid solution layer may be due to a chemical reaction from the interface [36].

3.3. Microstructure of the interface

Fig. 3(a) shows the TEM micrographs of joined interface of SUS304 and MG. In the middle part of the figure, the bright area represented by the blue dotted line is the joint between SUS304 and MG. It is a smooth transition zone without any cracks, holes, or pores which reveals a highquality bonding between them. The two sides of the joined region differ noticeably in terms of morphology because they belong to different materials SUS304 and MG respectively. The top half of the image marked "SUS304" represents this area is the SUS304 matrix, although it shows a rough surface visually, the atoms are all long-range ordered in a crystalline state. The inset in the upper left corner was a selected area electron diffraction (SEAD) belonging to that region. These symmetrical bright spots confirmed the face-centered cubic structure austenite phase again. The low half of the image shows a different matrix marked "MG", this area is a Cu₄₆Zr₄₆Al₈ matrix obtained by rapid cooling of molten liquid, and most atoms are distributed in long-range disordered arrangements. The same inset in the bottom right corner is a SEAD belonging to this region. The main part of SEAD shows a hollow ring which represents an amorphous structure of this area, however, around the hollow ring, there are still some asymmetrical and scattered spots marked by white circles, which indicate the presence of nanocrystals.

An enlarged high-resolution TEM image from the joint is shown in Fig. 3(b), several nanocrystal particles with a diameter of 2–3 nm can be observed from the MG side at the edge of joined region, given the fact that MG partial crystallization observed and the nanocrystals are generated at the glass phase. Previous studies have proved that this phenomenon is common in the dissimilar joining of metallic glass [37, 38]. The size of these nanocrystal is sensitive to the cooling rates, if sufficient cooling rate can be provided, these small particles will disappear, otherwise, their size will be larger. In this study, the joined region is situated in the middle of the cylinder, 1 mm away from the copper mold's edge, moreover, the inserted SUS304's thermal conductivity is not as good as the copper mold, these two reasons can affect the cooling rate of molten metal in the same time. However, these generated 2–3 nm nanocrystals will not influence the joining quality, it has been

reported that the existence of nanocrystals in the MG matrix even can break the trade-off relationship between plasticity and strength [39]. Fig. 3(c) shows an enlarged high-resolution TEM image from the interface framed by a yellow box in Fig. 3(b), this is the atomic-scale micro-structure transitioning from the SUS304 matrix to the joined zone, there is a distinct boundary between two different matrices, as indicated by the blue dashed line, it demonstrates atomic-level metallurgical bonding between them. The enlarged joined zone shows no crystals visible in it, and the atoms exhibit a completely disordered form, that means the interface of MG and stain steel is totally an amorphous phase. Although the atoms from the MG side are also disordered, there is also a clear interface between the two amorphous matrices as demonstrated in Fig. 3(b). This phenomenon might be well explained by elemental polymerization, the MG side only contains 3 elementals Cu, Zr, and Al, but diffusion of elements occurred in the joined region, meaning that except the three MG elementals, Cr, Fe, and Ni from SUS304 were also existed. This difference in elemental species creating a distinct interface [40], causes the forming of distinct lines between the two amorphous phases in the image.

3.4. The mechanism of liquid-solid casting

Combined with the results and discussion above, the mechanism of this liquid-solid casting process between SUS304 and MG might be explained as Fig. 4(a-c) shown, the whole process can be divided into three steps, the first step is shown in Fig. 4(a), even though the surface of SUS304 has been carefully polished, but a rough surface inevitably exists. On the other hand, the melting point of SUS304 is about 1671–1721 K [41]. However, zirconium, as a component in MG, it's melting point is about 2125 K [42], so the temperature of the molten metal liquid at least higher than 2125 K. When the high-temperature liquid metal contacts with SUS304, the process comes into the second step as shown in Fig. 4 (b). A small melting zone forms between the liquid metal and the rough surface, because the temperature of the liquid metal is higher than the melting point of SUS304 at the moment, resulting in the diffusion of elements near the interface. Moreover, the process was conducted in air, oxides are inevitably formed during the cooling process, which is proved by the large enrichment of oxygen elements in EDS in Fig. 2(a). Benefit from the whole process was conducted in a copper mold, rapid cooling can be reached. As illustrated in Fig. 4(c), except for a little nanocrystal measured about 2-3 nm along the joined region from the MG side, amorphous structures are formed from rapid cooling. However, the melting zone, atomically strong metallurgical bonding is accomplished when the bond is exposed to air and reacts with oxygen to generate a stable oxide when cooled. Kuroda et al. [43] also found similar phenomenon when weld super duplex stainless steel with Zr-based metallic glass by using micro flash butt welding, the success of welding mainly relies on Zr-based metallic glass become liquid phase during heating.

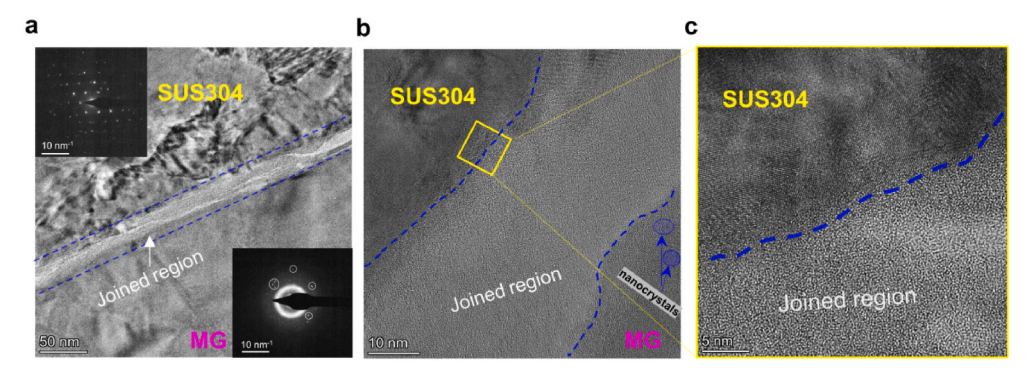


Fig. 3. (a) TEM micrographs of the joined interface of SUS304 and MG, the inset was selected area electron diffraction (SEAD) belonging to each region. (b) Enlarged view of the interface. (c) Enlarged view of the area framed by yellow box in (b). (For interpretation of the references to color in this figure legend, the reader is referred to the Web version of this article.)

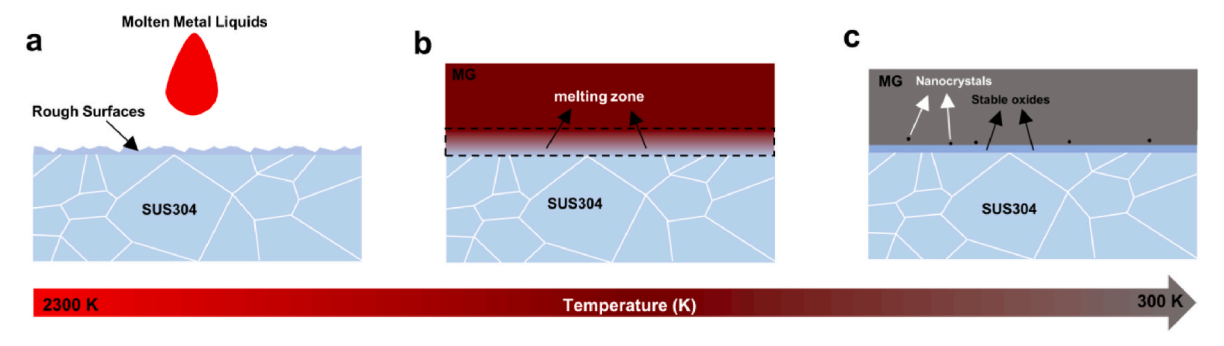


Fig. 4. (a-c) Schematic diagram of this solid-liquid casting mechanism between SUS304 and MG.

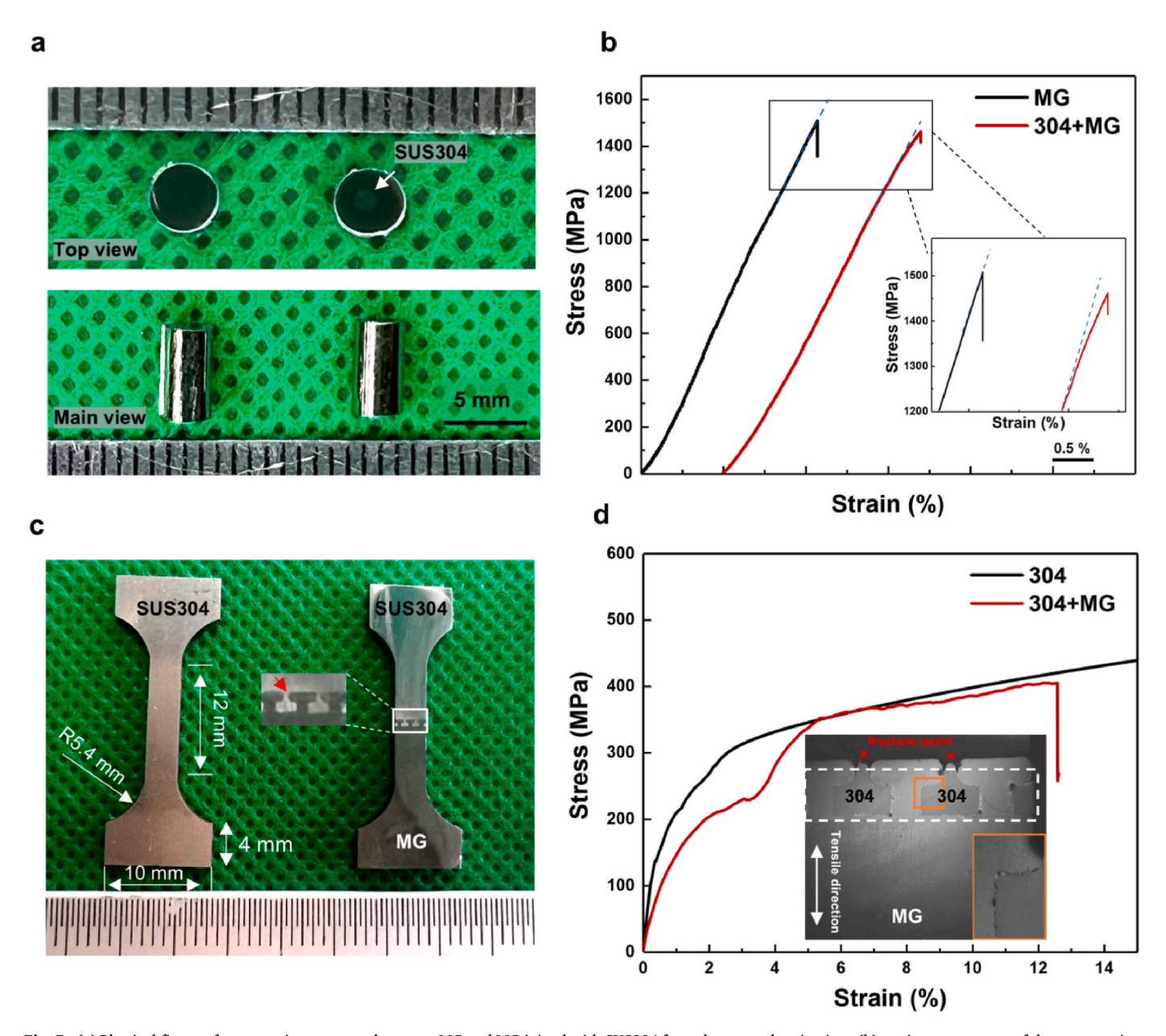


Fig. 5. (a) Physical figure of compression test sample as-cast MG and MG joined with SUS304 from the top and main view. (b) strain-stress curves of the compression tests, the inset was the partial enlargement of the black boxed area. (c) Photos of tensile test sample SUS304 and MG joined with SUS304. (d) strain-stress curves of tensile tests, the inset is the fractured morphology near the joint.

3.5. Mechanical tests of joined sample

In addition, mechanical tests were conducted to assess the quality of this liquid-solid casting method. As shown in Fig. 5(a), there is a photo of two compression samples from the top view and main view, the left one is pure MG, the right one is MG and SUS304 joined together, a SUS304 with a diameter of 1 mm indicated by a white arrow was joined in the center. Two strain-stress curves are shown in Fig. 5(b), due to the disordered atomic structure, plastic deformation cannot be achieved by dislocations and twins [44], thus sudden brittle fracture occurs in the elastic phase, achieving a maximum compressive strength of 1512 MPa. On the other hand, the MG joined with the SUS304 sample shows a compressive strength of 1461 MPa, numerically 97 % of as cast MG sample.

As is well known, compressive properties of metallic glass sensitive to defects and holes in the matrix [45], a single point of stress concentration can drive a catastrophic brittle fracture, similar compression strength benefits from the well-joined interface of MG and SUS 304, metallurgical bonding is tight without gaps or cracks at the atomic level at the joint. Moreover, the compression curves of the samples before fracture are magnified in the inset of Fig. 5(b), the dotted line is an extension made along the slope of the curve, one can see that brittle fracture occurred during the elastic phase in as-cast MG, however, a small period of yielding occurs at the end of elasticity in MG joined with SUS304 sample. Although the enhanced plasticity is limited because SUS304 is centralized in the center of the sample and only occupies 11.1 % of the sample volume. Through some rational design, this liquid-solid casting method is not only a useful joining strategy but also a novel strategy to manufacture composite materials with excellent properties. It has been reported that using a similar way to combine Ti-based MG with Cu foam can enhance plasticity from 2.5 % to 5.6 % [46].

In addition, tensile strength was also evaluated, Fig. 5(c) shows typical dog bone-shaped tensile specimens of SUS304 and SUS304 joined with MG, the inset was a partial enlargement of joint between SUS304 and MG, this is a structure consisting of multiple T-slots, liquid metal flows into the groove for joining and self-locking. Since MG is significantly stronger than stainless steel [47], stainless steel will show plastic deformation before MG due to its inability to withstand large tensile forces, which is why pure stainless steel was selected as the comparative material. The thickness of the specimen is 1.5 mm and other dimensional parameters are demonstrated in the figure. The strain-stress curves of the tensile experiment are shown in Fig. 5(d), the joined sample reached a tensile strength of 404 MPa before fracture and had a strain of about 12.6 %, the curve shows the same trend as pure SUS304, which means the self-locking is strong enough to reach maximum yield strength withstand elastic stage, and the SUS304 occurs plastic deformation with strain 12.5 % before failure, the failure location is the groove of the T-slot on the SUS 304 side indicated by the red arrow in Fig. 5(c), the inset of Fig. 5(d) is the fractured morphology near the joint, the fractured point is in the SUS304 part, as enlarged interface of MG and SUS 304 in the orange box shown, the MG and SUS 304 still joined well with each other after tensile, that means the joint quality is strong enough, so SUS 304 fractured before the joint fractured. if the quality of joint is not good, the joint will move along the direction perpendicular to the tensile test. by changing the shape and size of the interface, higher connection strengths are also possible. Therefore, through proper design, this liquid-solid casting technology can be used to connect MG with other steels with reliable bond strength.

However, there are still some issues need to consider in our approach. One is the metastable of metallic glass, the amorphous structure is trend to crystallize over time, this will decrease the reliability of joint, but a higher cooling rate can delay the occurrence of this phenomenon. Another is residual stresses, the rapid cooling of high-temperature liquids inevitably results in residual stresses, this may lead to brittle failure of the joint, low-temperature annealing can be considered to enhance the performance of the joint.

4. Conclusion

In this work, by using a liquid-solid casting method, we successfully joined Zr-based MG and SUS304 together as a single unit. A metallurgically bonded interface without any cracks or cavities was obtained. The elemental diffusion zone with a thickness of approximately 40 nm suggests it is a kind of melt joining, so it requires the melting point of the steels to be joined at least 100–150 K lower than the molten metal liquid. The joined region between MG/SUS304 shows atomic long-range disorder and accompanying large enrichment of oxygen, which indicates the presence of stable oxides in the transition zone. The joined sample reaches 97 % compression strength as as-cast MG up to 1461 MPa, moreover, with a strain of 12.6 %, the tensile strength can reach 404 MPa before breaking. Our results demonstrated this is an easy and economical way to join MG and steels, and the quality of the joining is reliable. The shape of the material to be joined is not limited, Therefore, it can be flexibly designed according to the application scenario.

CRediT authorship contribution statement

Yu Zhang: Writing – original draft, Methodology, Data curation, Conceptualization. Luyao Li: Software, Formal analysis. Xin Li: Data curation. Wenxin Wen: Software. Yong Xiao: Writing – review & editing, Supervision, Resources. Dan Li: Formal analysis. Jiang Ma: Writing – review & editing, Supervision, Resources, Funding acquisition.

Declaration of competing interest

The authors declare that they have no known competing financial interests or personal relationships that could have appeared to influence the work reported in this paper.

Acknowledgments

The work was financially supported by the Key Basic and Applied Research Program of Guangdong Province, China [Grant No. 2019B030302010], the Science and Technology Innovation Commission Shenzhen [Grants No. RCJC20221008092730037, 20220804091920001]. The authors also thank the assistance on microscope observation received from the Electron Microscope Center of Shenzhen University.

Data availability

Data will be made available on request.

References

- S. Xu, X. Jing, P. Zhu, H. Jin, K.-W. Paik, P. He, S. Zhang, Equilibrium phase diagram design and structural optimization of SAC/Sn-Pb composite structure solder joint for preferable stress distribution, Mater. Char. 206 (2023) 113389. https://10.1016/j.matchar.2023.113389.
- [2] J. Wang, Y. Xie, X. Meng, Y. Zhao, S. Sun, J. Li, J. Chen, H. Chen, X. Ma, N. Wang, Y. Huang, Wire-based friction stir additive manufacturing towards isotropic high-strength-ductility Al-Mg alloys, Virtual Phys. Prototyp. 19 (2024). https:// 10.1080/17452759.2024.2417369.
- [3] Z. Wang, Y. Xiang, S. Zhang, X. Liu, J. Ma, J. Tan, L. Wang, Physics-informed springback prediction of 3D aircraft tubes with six-axis free-bending manufacturing, Aero. Sci. Technol. 147 (2024) 109022, https://doi.org/10.1016/j. ast.2024.109022.
- [4] M. Huang, L. Wang, C. Wang, Y. Li, J. Wang, J. Yuan, J. Hu, M. Huang, W. Xu, Optimizing crack initiation energy in austenitic steel via controlled martensitic transformation, J. Mater. Sci. Technol. 198 (2024) 231–242, https://doi.org/ 10.1016/j.imst.2024.02.019.
- [5] M.X. Li, S.F. Zhao, Z. Lu, A. Hirata, P. Wen, H.Y. Bai, M. Chen, J. Schroers, Y. Liu, W.H. Wang, High-temperature bulk metallic glasses developed by combinatorial methods, Nature 569 (2019) 99–103. https://10.1038/s41586-019-1145-z.
- [6] J. Brechtl, Z. Wang, X. Xie, J.-W. Qiao, P.K. Liaw, Relation between the defect interactions and the serration dynamics in a Zr-based bulk metallic glass, Appl. Sci. 10 (2020) 3892. https://10.3390/app10113892.

- [7] S. Sohrabi, J. Fu, L. Li, Y. Zhang, X. Li, F. Sun, J. Ma, W.H. Wang, Manufacturing of metallic glass components: processes, structures and properties, Prog. Mater. Sci. 144 (2024) 101283, https://doi.org/10.1016/j.pmatsci.2024.101283.
- [8] X. Li, L. Li, S. Sohrabi, J.n. Fu, Z. Li, Z. Chen, R. Sun, Y. Zhang, J. Huang, H. Zhang, J. Zhu, X. Chen, K. Song, J. Ma, Ultrasonic vibration enabled under-liquid forming of metallic glasses, Sci. Bull. 69 (2024) 163–166, https://doi.org/10.1016/j.cgib.2023.11.049
- [9] Y. Zhang, S. Sohrabi, X. Li, S. Ren, J. Ma, Tailored gradient nanocrystallization in bulk metallic glass via ultrasonic vibrations, J. Mater. Sci. Technol. 210 (2025) 109–120, https://doi.org/10.1016/j.jmst.2024.05.027.
- [10] Y. Yang, N. Hua, R. Li, S. Pang, T. Zhang, High-zirconium bulk metallic glasses with high strength and large ductility, Sci. China Phys. Mech. Astron. 56 (2013) 540–544. https://10.1007/s11433-013-5015-7.
- [11] L. Hua, Y. Liu, D. Qian, L. Xie, F. Wang, M. Wu, Mechanism of void healing in cold rolled aeroengine M50 bearing steel under electroshocking treatment: a combined experimental and simulation study, Mater. Char. 185 (2022) 111736, https://doi. org/10.1016/j.matchar.2022.111736.
- [12] F. Wang, A. Inoue, F. Kong, S. Zhu, C. Xie, C. Zhao, W.J. Botta, C. Chang, Formation and ultrahigh mechanical strength of multicomponent Co-based bulk glassy alloys, J. Mater. Res. Technol. 26 (2023) 1050–1061. https://10.1016/j.jmrt.2023.0
- [13] X. Li, J. Zhou, L. Shen, B. Sun, H. Bai, W. Wang, Exceptionally high saturation magnetic flux density and ultralow coercivity via an amorphous–nanocrystalline transitional microstructure in an FeCo-based alloy, Adv. Mater. (2022). https://10. 1002/adma.20205863
- [14] Y. Zhang, S. Ren, S. Sohrabi, J. Ma, Primary and secondary phase separation in Cu–Zr–Al bulk metallic glass by control of quenching conditions, Intermetallics 156 (2023) 107853, https://doi.org/10.1016/j.intermet.2023.107853.
- [15] G. Zhang, W. Sun, L. Xie, C. Zhang, J. Tan, X. Peng, Q. Li, X. Ma, D. Zhao, J. Yu, Multicomponent Fe-based bulk metallic glasses with excellent corrosion and wear resistances, Metals 12 (2022) 564. https://10.3390/met12040564.
- [16] X.S. Wei, J.L. Jin, Z.Z. Jiang, D.D. Liang, J. Shen, FeCrMoWCBY metallic glass with high corrosion resistance in molten lead–bismuth eutectic alloy, Corrosion Sci. 190 (2021) 109688. https://10.1016/j.corsci.2021.109688.
- [17] A. de Pablos-Martín, T. Höche, Laser welding of glasses using a nanosecond pulsed Nd:YAG laser, Opt Laser. Eng. 90 (2017) 1–9, https://doi.org/10.1016/j. optlaseng.2016.09.009.
- [18] N.H. Tariq, M. Shakil, B.A. Hasan, J.I. Akhter, M.A. Haq, N.A. Awan, Electron beam brazing of Zr62Al13Ni7Cu18 bulk metallic glass with Ti metal, Vacuum 101 (2014) 98–101, https://doi.org/10.1016/j.vacuum.2013.07.010.
- [19] Y. Yang, J. Kong, K. Dong, Q. Wang, S. Feng, Y. Liang, X. Chen, X. Liu, Joining of dissimilar bulk metallic glasses with non-common supercooled liquid regions, Mater. Sci. Eng. 864 (2023) 144608, https://doi.org/10.1016/j. msea 2023 144608
- [20] B.W. Seo, Y.C. Jeong, H.J. Son, C.J. Kim, S. Kim, Y.T. Cho, Application of synchronized tandem welding to high-hardness armor steel, Heliyon 10 (2024) e24257, https://10.1016/j.heliyon.2024.e24257.
- [21] X. Li, X. Liang, Z. Zhang, J. Ma, J. Shen, Cold joining to fabricate large size metallic glasses by the ultrasonic vibrations, Scripta Mater. 185 (2020) 100–104. https://10.1016/j.scriptamat.2020.03.059.
- [22] Y. Kawamura, T. Shoji, Y. Ohno, Welding technologies of bulk metallic glasses, J. Non-Cryst. Solids 317 (2003) 152–157, https://doi.org/10.1016/S0022-3093 (20202005 7
- [23] W. Zhang, X. Yang, J. Lin, B. Lin, Y. Huang, Experimental and numerical study on the torsional behavior of rectangular hollow reinforced concrete columns strengthened by CFRP, Structures 70 (2024) 107690, https://doi.org/10.1016/j. istruc.2024.107690
- [24] Y. Zhao, Integrated unified phase-field modeling (UPFM), Materials Genome Engineering Advances 2 (2024). https://10.1002/mgea.44.
- [25] H. Li, Z. Li, J. Yang, H.B. Ke, B. Sun, C.C. Yuan, J. Ma, J. Shen, W.H. Wang, Interface design enabled manufacture of giant metallic glasses, Sci. China Mater. 64 (2021) 964–972. https://10.1007/s40843-020-1561-x.
- [26] J. Ma, C. Yang, X. Liu, B. Shang, Q. He, F. Li, T. Wang, D. Wei, X. Liang, X. Wu, Fast surface dynamics enabled cold joining of metallic glasses, Sci. Adv. 5 (2019) eaax7256. https://10.1126/sciadv.aax7256.
- [27] Z. Huang, J. Fu, X. Li, W. Wen, H. Lin, Y. Lou, F. Luo, Z. Zhang, X. Liang, J. Ma, Ultrasonic-assisted rapid cold welding of bulk metallic glasses, Sci. China Mater. 65 (2021) 255–262. https://10.1007/s40843-021-1723-6.

- [28] L. Li, X. Li, Z. Huang, J. Huang, Z. Liu, J. Fu, W. Wen, Y. Zhang, S. Huang, S. Ren, J. Ma, Joining of metallic glasses in liquid via ultrasonic vibrations, Nat. Commun. 14 (2023). https://10.1038/s41467-023-42014-x.
- [29] J. Cao, H.Y. Chen, X.G. Song, J.K. Liu, J.C. Feng, Effects of Ar ion irradiation on the diffusion bonding joints of Zr55Cu30Ni5Al10 bulk metallic glass to aluminum alloy, J. Non-Cryst. Solids 364 (2013) 53–56, https://doi.org/10.1016/j. inoncrysol.2013.01.012.
- [30] J. Kim, Y. Kawamura, Dissimilar welding of Zr41Be23Ti14Cu12Ni10 bulk metallic glass and stainless steel, Scripta Mater. 65 (2011) 1033–1036. https://10.1016/j. scriptamat.2011.06.032.
- [31] A. Chen, J. Liu, H. Wang, J. Lu, Y.M. Wang, Gradient twinned 304 stainless steels for high strength and high ductility, Mater. Sci. Eng. 667 (2016) 179–188. https://10.1016/j.msea.2016.04.070.
- [32] L. Hua, Y. Du, D. Qian, M. Sun, F. Wang, Influence of prior cold rolling on bainite transformation of high carbon bearing steel, Metall. Mater. Trans. 56 (2025) 640–654. https://10.1007/s11661-024-07669-1.
- [33] H.S. Yun, S.K. Jeon, Y.-K. Lee, J.S. Park, S.H. Nahm, Effect of precharging methods on the hydrogen embrittlement of 304 stainless steel, Int. J. Hydrogen Energy 50 (2024) 175–188, https://doi.org/10.1016/j.ijhydene.2023.09.073.
- [34] J.H. Kong, M. Okumiya, Y. Tsunekawa, K.Y. Yun, S.G. Kim, M. Yoshida, A novel bonding method of pure aluminum and SUS304 stainless steel using barrel nitriding, Metall. Mater. Trans. 45 (2014) 4443–4453. https://10.1007/s11661-0 14-2380-4
- [35] J. Kim, T. Lee, Brazing method to join a novel Cu54Ni6Zr22Ti18 bulk metallic glass to carbon steel, Sci. Technol. Weld. Join. 22 (2017) 714–718. https://10.1080/13 621718 2017 1306155
- [36] A. Saadati, M. Malekan, F. Khodabakhshi, Under glass transition temperature diffusion bonding of bulk metallic glass and aluminum, Mater. Chem. Phys. 269 (2021) 124758, https://doi.org/10.1016/j.matchemphys.2021.124758.
- [37] A. Saadati, M. Malekan, F. Khodabakhshi, G. Wilde, A.P. Gerlich, Dissimilar diffusion bonding of bulk metallic glass: amorphous/crystalline atomic-scale interaction, Mater. Char. 195 (2023) 112480, https://doi.org/10.1016/j. matchar.2022.112480.
- [38] C. Wen, T. Shi, B. Chen, Z. Zhu, Y. Peng, G. Liao, Diffusion bonding of Zr55Cu30Ni5Al10 bulk metallic glass to Cu with Al as transition layer, Mater. Des. 83 (2015) 320–326, https://doi.org/10.1016/j.matdes.2015.06.028.
- [39] W. Zhai, L.H. Nie, X.D. Hui, Y. Xiao, T. Wang, B. Wei, Ultrasonic excitation induced nanocrystallization and toughening of Zr46.75Cu46.75Al6.5 bulk metallic glass, J. Mater. Sci. Technol. 45 (2020) 157–161. https://10.1016/j.jmst.2019.10.035.
- [40] Y. Zhang, S. Ren, S. Sohrabi, J. Ma, Primary and secondary phase separation in Cu–Zr–Al bulk metallic glass by control of quenching conditions, Intermetallics 156 (2023). https://10.1016/j.intermet.2023.107853.
- [41] T. Sumita, T. Kitagaki, M. Takano, A. Ikeda-Ohno, Solidification and re-melting mechanisms of SUS-B4C eutectic mixture, J. Nucl. Mater. 543 (2021) 152527, https://doi.org/10.1016/j.jnucmat.2020.152527.
- [42] P. Parisiades, F. Cova, G. Garbarino, Melting curve of elemental zirconium, Phys. Rev. B 100 (2019) 054102, https://doi.org/10.1103/PhysRevB.100.054102.
- [43] T. Kuroda, M. Shimada, Micro flash butt welding of super duplex stainless steel with Zr-based metallic glass insert, Vacuum 83 (2008) 153–156. https://10.1016/j. vacuum.2008.03.089.
- [44] Y. Wu, B. Deng, X. Li, Q. Li, T. Ye, S. Xiang, M.-C. Zhao, A. Atrens, In-situ EBSD study on twinning activity caused by deep cryogenic treatment (DCT) for an as-cast AZ31 Mg alloy, J. Mater. Res. Technol. 30 (2024) 3840–3850, https://doi.org/10.1016/j.imrt.2024.04.099.
- [45] F. Li, Z. Zhang, H. Liu, W. Zhu, T. Wang, M. Park, J. Zhang, N. Bönninghoff, X. Feng, H. Zhang, J. Luan, J. Wang, X. Liu, T. Chang, J.P. Chu, Y. Lu, Y. Liu, P. Guan, Y. Yang, Oxidation-induced superelasticity in metallic glass nanotubes, Nat. Mater. 23 (2024) 52–57. https://10.1038/s41563-023-01733-8.
- [46] H. Wang, R. Li, Y. Wu, X.M. Chu, X.J. Liu, T.G. Nieh, Z.P. Lu, Plasticity improvement in a bulk metallic glass composed of an open-cell Cu foam as the skeleton, Compos. Sci. Technol. 75 (2013) 49–54. https://10.1016/j.compscit ech. 2012 11 017
- [47] T. Yamamoto, H. Kasahara, R. Aoki, E. Miura, Resistance spot welding of stainless steel and titanium plates with a supercooled liquid of Zr55Al10Ni5Cu30 metallic glass ribbons, Metall. Mater. Trans. 55 (2024) 2589–2595. https://10.1007 /s11661-024-07432-6.